FOCUS

COVID-CheXNet: hybrid deep learning framework for identifying COVID-19 virus in chest X-rays images

Alaa S. Al-Waisy[1] · Shumoos Al-Fahdawi[2] · Mazin Abed Mohammed[3] · Karrar Hameed Abdulkareem[4] · Salama A. Mostafa[5] · Mashael S. Maashi[6] · Muhammad Arif[7] · Begonya Garcia-Zapirain[8]

Abstract

The outbreaks of Coronavirus (COVID-19) epidemic have increased the pressure on healthcare and medical systems worldwide. The timely diagnosis of infected patients is a critical step to limit the spread of the COVID-19 epidemic. The chest radiography imaging has shown to be an effective screening technique in diagnosing the COVID-19 epidemic. To reduce the pressure on radiologists and control of the epidemic, fast and accurate a hybrid deep learning framework for diagnosing COVID-19 virus in chest X-ray images is developed and termed as the COVID-CheXNet system. First, the contrast of the X-ray image was enhanced and the noise level was reduced using the contrast-limited adaptive histogram equalization and Butterworth bandpass filter, respectively. This was followed by fusing the results obtained from two different pre-trained deep learning models based on the incorporation of a ResNet34 and high-resolution network model trained using a large-scale dataset. Herein, the parallel architecture was considered, which provides radiologists with a high degree of confidence to discriminate between the healthy and COVID-19 infected people. The proposed COVID-CheXNet system has managed to correctly and accurately diagnose the COVID-19 patients with a detection accuracy rate of 99.99%, sensitivity of 99.98%, specificity of 100%, precision of 100%, F1-score of 99.99%, MSE of 0.011%, and RMSE of 0.012% using the weighted sum rule at the score-level. The efficiency and usefulness of the proposed COVID-CheXNet system are established along with the possibility of using it in real clinical centers for fast diagnosis and treatment supplement, with less than 2 s per image to get the prediction result.

Keywords Coronavirus COVID-19 epidemic · Deep learning · Transfer learning · ResNet34 model · Chest radiography imaging · Chest X-ray images

✉ Alaa S. Al-Waisy
king_alaa87@yahoo.com

Shumoos Al-Fahdawi
sun_algold@yahoo.com

Mazin Abed Mohammed
mazinalshujeary@uoanbar.edu.iq

Karrar Hameed Abdulkareem
khak9784@mu.edu.iq

Salama A. Mostafa
salama@uthm.edu.my

Mashael S. Maashi
mmaashi@ksu.edu.sa

Muhammad Arif
arifmuhammad36@hotmail.com

Begonya Garcia-Zapirain
mbgarciazapi@deusto.es

Extended author information available on the last page of the article

1 Introduction

The Coronavirus (COVID-19) epidemic is one of the most infectious diseases, which is distinguished as a pandemic due to its ability to rapidly spread in most of the world countries with serious effects on the lives of billions of people. The first COVID-19 infected case was identified in December 2019 in Wuhan city. Recently, all the countries around the world are striving and fighting to limit the spread of the COVID-19 epidemic. To date, the number of positive confirmed COVID-19 cases worldwide is around 34,170,335 cases and 1,018,899 death cases, and 25,437,901 were recovered (Worldmeter 2020). As shown in Fig. 1, the number of daily confirmed infected cases is dramatically increasing, while it was less than 500 cases, on February 2, 2020, it is exceeding the 315,710 confirmed cases, on September 30, 2020. In contrast, the highest number of recovered cases was 298,473 cases, on

September 18, 2020. Most of the people who are infected with COVID-19 are suffering from a respiratory disease that does not require special treatment. The elderly and those with chronic diseases, such as diabetes chronic respiratory disease, cancer identification, cardiovascular disease detection, and chronic respiratory disease are more likely to experience dangerous illness (Chen et al. 2020). Some critical symptoms can be recognized on the infected COVID-19 patient, such as fever, dry cough, tiredness, headache, vomiting, sore throat, sneezing, dyspnea, and myalgia (Huang et al. 2020; Guo et al. 2020). To date, there is no unique drug or vaccine available for the COVID-19 virus where several extensive clinical trials and experiments were conducted to find new therapies.

The most important step to monitor and control the COVID-19 virus rapid spread is employing an efficient screening technique for infected patients to enable the early diagnosis of the virus and patient treatment follow-up. Until now, many screening techniques have been employed to detect the initial symptoms of the COVID-19 virus. For instance, polymerase chain reaction (PCR) is a commonly used screening technique to identify SARS-CoV-2 RNA from respiratory samples as well as the COVID-19 virus (Wang et al. 2020a, b). Although, the high sensitivity of the PCR testing, it is considered as a very tedious and time-consuming technique and required more user interaction. To overcome these limitations of the PCR technique, several studies have demonstrated the reliability of the chest radiography imaging technique, such as the X-ray and computed tomography (CT) in early diagnosis of the COVID-19 virus (Ming-Yen et al. 2020). For instance, CT findings were positive for 140 patients with COVID-19 infection as presented in (Huang et al. 2020). Thus, chest radiographs imaging technique is considered as one of the most powerful medical imaging techniques in the hospital to detect chest abnormalities. However, the major issue of using the chest radiograph imaging technique is the long-time required by the radiologists to read and interpret the chest radiography images (Brady 2017). Furthermore, since the COVID-19 virus was reported as a pandemic, the number of patients who required an X-ray image examination is increasing compared with a fewer number of available radiologists. Consequently, this can keep the radiologists and the hospital overloaded, delay the diagnosis process, and affect patient's treatment and follow-up, and a serious risk of cross-infection to other people. Therefore, the need for a rapid and automated interpretation of the radiography images to help the radiologists to accurately detect the COVID-19 virus is extremely desired. To overcome these drawbacks of the adopted imaging acquisition techniques and enhance the image quality, computer-aided diagnostic (CAD) system can be used to help radiologists and clinicians correctly interpreting and understanding the details of a massive amount of chest radiography images in real-time.

This paper proposes a new hybrid deep learning framework, named as the COVID-CheXNet system for diagnosing COVID-19 virus in X-ray images by combining the results obtained from two discriminative deep learning models. The proposed COVID-CheXNet system is composed of four main stages: image pre-processing, features extraction, image classification, and fusion. First, the CLAHE method and Butterworth bandpass filter are applied sequentially to enhance the contrast of the chest X-ray image and reduce the noise level, respectively. This is followed by applying two distinctive deep learning approaches based on ResNet34 and HRNet to address the features extraction and classification tasks in the proposed
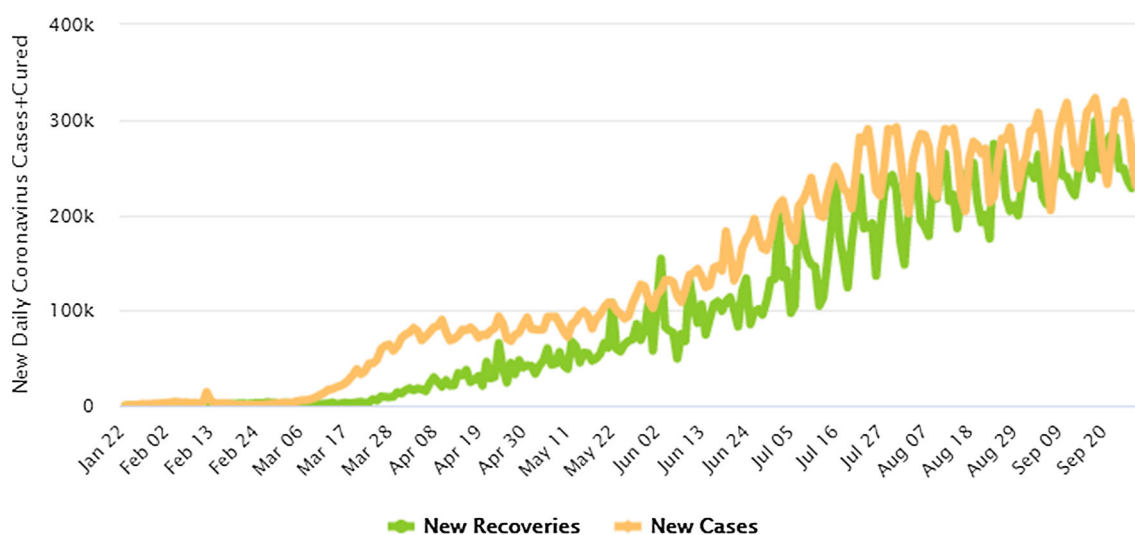

Fig. 1 The plots of the number of newly infected versus the number of recovered and discharged patients each day (Worldmeter 2020)

COVID-CheXNet system. Finally, the results generated from these two deep learning models are combined to make the final decision. The main motivation of developing the proposed COVID-CheXNet system is to employ it as a diagnostic tool that can help the decision-makers in the medical and health centers (radiologists and clinicians) to rapidly and accurately identify the COVID-19 virus in the X-ray images. This can significantly reduce the pressure on the radiologists and hospitals while this epidemic is still rapidly spreading and the number of infected people is dramatically increased. The main contributions of this study can be summarized as follows:

1. A new hybrid deep learning framework is proposed, termed as the COVID-CheXNet system for diagnosing COVID-19 pneumonia in chest X-rays images by combining the results generated from two different deep learning methods (e.g., ResNet34 and HRNet). To the authors' best knowledge, this is the first attempt to examine the possibility of using ResNet34 and HRNet models in a unified system to detect the COVID-19 virus in X-ray images. Furthermore, no one as far as we know has applied the HRNet for diagnosing the COVID-19 virus in X-ray images. Unlike most of the previously existing systems, the final decision in the proposed COVID-CheXNet system is obtained by combining the results generated from two different deep learning models trained on the top of a large-scale and challenging dataset. Herein, a high degree of confidence is given to radiologists to differentiate between healthy and COVID-19 infected cases by considering the parallel architecture to combine the results obtained.

2. An efficient image enhancement procedure is proposed based on the CLAHE method and Butterworth band-pass filter to enhance the contrast of the X-ray image and reduce the noise level, respectively. We argue that training the adopted deep learning models on the top of the pre-processing images data instead of direct usage of raw data can significantly enhance their ability to learn more useful feature representations with less computational complexity to obtain the best-trained model.

3. A discriminative training methodology supported by a set of different training strategies (e.g., data augmentation, dropout method, etc.) is also adopted to further improve the generalization ability of the adopted deep learning models and prevent the overfitting problem during the learning process.

4. A large-scale and challenging X-ray dataset is created and termed as the COVID19-vs-normal dataset. To the authors' best knowledge, this dataset is the largest COVID-19 dataset currently available in the public domain in terms of containing the largest amount of X-ray images with confirmed COVID-19 infection.

5. Establish an efficient and useful system that can be employed in a real-world clinical situation for fast diagnosis and treatment follow-up that consume less than 2 s per image to produce the final results.

This paper is organized as follows: Sect. 2 provides a brief overview of the current related works. The strategy used to create the COVID19-vs-normal dataset and the implementation details of the COVID-CheXNet system are discussed in Sect. 3. Experimental results are presented in Sect. 4. In Sect. 5, the conclusion of this study and future work are provided.

2 Related works

Deep learning networks (DNNs) have been efficiently employed in the medical field with remarkable results and significant performance compared with the human-level performance in various challenging image analysis and classification tasks (Al-Waisy et al. 2017a, b, 2018). Several medical imaging systems based on deep learning approaches have also been employed to support the clinicians in the early detection of COVID-19 infection, treatment, and follow-up investigation (De Fauw et al. 2018). For instance, Ozturk et al. (2020) proposed an automated COVID-19 detection system based on the DarkNet model to perform a binary classification task (e.g., normal and COVID-19) and a multiclass classification task (e.g., normal, pneumonia, and COVID-19). This system has managed to achieve up to 98.08% accuracy. A tailored COVID-Net model for detecting the virus by using chest X-ray images was developed by Wang and Wong (2020). The COVID-Net model was trained to categorize the chest X-ray image into one of three different classes (e.g., normal, none-COVID19, and COVID19). The performance of the COVID-Net model was tested using a dataset comprises a total of 16,756 images gathered from two different datasets (COVID-19 X-ray dataset presented in Cohen et al. (2020) and RSNA pneumonia detection challenge dataset (2020). The highest accuracy rate of 92.4% was achieved. Hemdan et al. (2020) developed a deep learning model, termed as COVIDX-Net to diagnose the COVID-19 virus through the analysis of chest X-ray images. The authors have tested the performance of seven diverse pre-trained models (e.g., VGG19, DenseNet201, ResNetV2, Xception, Inception, InceptionV3, and MobileNetV2) using a relatively small dataset of 50 images (e.g., with 25 images with confirmed COVID-19 infection). The highest accuracy rate of 91% was achieved using the pre-trained DenseNet201 model. Narin et al. (2020) assessed the

performance of three pre-trained models (InceptionV3, ResNet50, and Inception-ResNetV2) using a small dataset consists of 100 X-ray images (e.g., 50 images of confirmed COVID-19 infection). The highest accuracy rate of 98% was obtained using the ResNet50 model. Mohammed and et al. (2020) developed a novel benchmarking method to choose the best COVID-19 detection model by using the Entropy and TOPSIS method and established a decision matrix of 10 evaluation criteria and 12 machine learning classifiers for identifying COVID-19 infection in 50 X-ray images. The highest closeness coefficient of 98.99% was achieved by the linear SVM classifier. Several convolutional neural network (CNN) models as feature descriptors were also trained by Kassani et al. (2020) to encode the input image into lower dimensional feature vectors. Then, these extracted feature vectors were fed into different classifiers to produce the final decision. Their performance has been tested using the same dataset presented in Cohen et al. (2020). The highest accuracy rate was 99% using the pre-trained DenseNet121 model as a features descriptor and the Bagging tree classifier. Zhang et al. (2020) employed a pre-trained ResNet18 model as a feature descriptor to extract discriminative features from the X-ray images. Then, these obtained features were processed by a multi-layer perception to produce the final decision. The highest accuracy rate of 96.00% was obtained using a dataset of 100 images captured from 70 patients with COVID-19 virus (Castillo and Melin 2020) developed a novel intelligent approach for forecasting COVID-19 time series by merging the advantages of the fractal dimension theory and fuzzy logic. In this hybrid approach, the linear and nonlinear fractal dimensions of the time series were fed into set of fuzzy rules to provide the forecast for the different countries based on their time series of confirmed COVID-19 infected and death cases. The proposed fuzzy model was built using a fixed period time series of 10 different countries, and then its reliability was tested using other periods of time series. The highest forecasting average accuracy of 98% was achieved. An interesting analysis of the spatial aspect of COVID-19 pandemic using unsupervised neural network, named as self-organizing maps, was presented by Melin et al. (2020). The authors proposed an efficient procedure using unsupervised self-organizing Kohonen maps to group together all the countries that have similar patterns of the COVID-19 cases. This procedure could be very helpful and essential in determining the best strategies for fighting against the COVID-19 epidemic in the countries that have similar patterns of infected COVID-19 cases. A comparison study between three different models (e.g., VGG-19, Inception_V2 and decision tree model) was presented by Dansana et al. (2020) to address the binary classification pneumonia task. Initially, the noise level in the input image was reduced using a feature detection kernel to generate compact feature maps. These feature maps were fed as input to the adopted deep learning models. The best accuracy rate of 91% was achieved using VGG-19 compared to 78% and 60% be achieved by Inception_V2 and decision tree model, respectively. Finally, other examples of applying different deep learning approaches for detecting COVID-19 virus can be found in Farooq and Hafeez (2020), Ghoshal and Tucker (2020), Kumar and Kumari (2020) and Gozes et al. 2020). This review on COVID-19 detection systems shows that most of the existing deep learning-based systems are limited to use the raw images data as an input to train the adopted deep learning models, which can affect the generalization ability of the last obtained model. Herein, we proposed to train the adopted deep learning models on the top of the pre-processing images data instead of direct usage of raw data to decrease the generalization error of the last trained model and avoid the overfitting issues. Furthermore, the performance of most of the existing systems has been validated using a very small dataset with a few images of COVID-19 infected cases, which is not sufficient to reveal the real performance of the proposed approaches. To overcome this limitation a large-scale and challenging dataset, termed as the COVID19-vs-normal dataset was created and used to evaluate the performance of the adopted deep learning models (See Sect. 3.1).

3 Proposed COVID-CheXNet system

In this section, a novel hybrid deep learning framework is proposed, termed as the COVID-CheXNet system for diagnosing COVID-19 virus in chest X-rays images by combining the results generated from two different deep learning methods (e.g., ResNet34 and HRNet). First, the adopted procedure to create the COVID19-vs-normal dataset is briefly described. Then, the implementation details of the proposed approaches are explained, including the proposed image enhancement procedure, the main architecture and training methodology of the employed deep learning models (e.g., ResNet34 and HRNet). Figure 2 shows the block diagram of the proposed COVID-CheXNet system for diagnosing COVID-19 virus in chest X-rays images.

3.1 COVID19-vs-normal dataset description

In this study, several X-ray images were carefully selected from different sources to create a relatively large-scale COVID-19 X-ray images dataset of confirmed infected cases. This dataset was termed as COVID19-vs-normal dataset and then mixed with some X-ray images of normal cases to be used for a more reliable diagnosis of COVID-19

Fig. 2 Block diagram of the proposed COVID-CheXNet system for diagnosing COVID-19 pneumonia in chest X-rays images
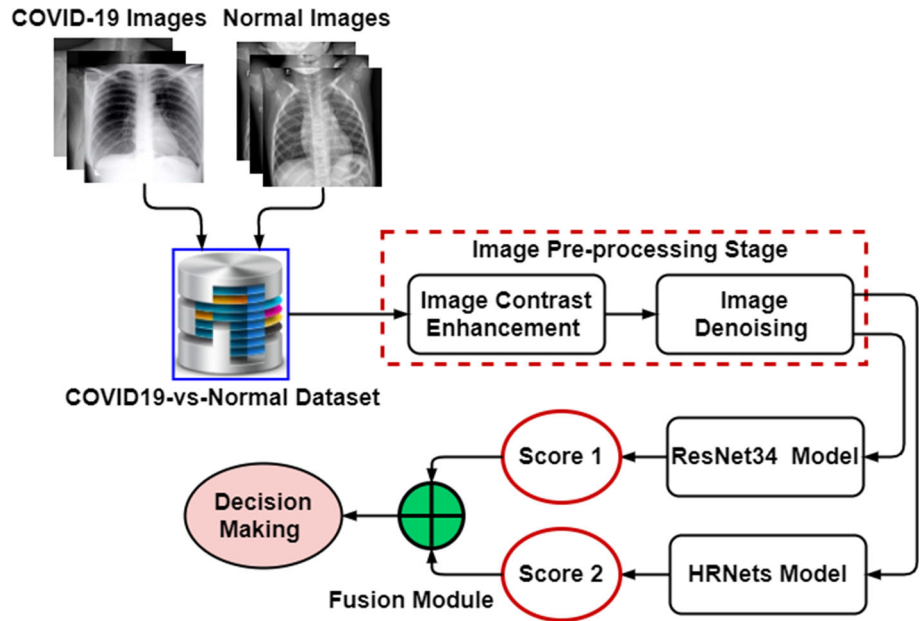
virus. The sources of the COVID19-vs-normal dataset are as follows:

- A number of 200 X-ray images with confirmed COVID-19 infection of Cohen's GitHub repository (Cohen et al. 2020).
- A number of 200 COVID-19 X-ray images with confirmed COVID-19 infection gathered from three different sources: Radiopaedia dataset (2020), Italian Society of Medical and Interventional Radiology (SIRM) (2020), and Radiological Society of North America (RSNA) (2020).
- A number of 400 chest X-ray images of normal condition was collected from Kaggle's chest X-ray images (Pneumonia) dataset (2020).

Samples of the COVID-19 and normal cases of the large-scale COVID-19 X-ray images are shown in Fig. 3. The number of the COVID-19 cases will continuously be updated accordingly with the availability of new X-ray images with confirmed COVID-19 infection, and the whole dataset is available publicly for academic research purposes at https://github.com/AlaaSulaiman/COVID19-vs-Normal-dataset. In this work, a data augmentation procedure was applied to avoid the overfitting problem and increase the generalization ability of the last trained model. Firstly, the size of the original image was rescaled to (224 × 224) pixels, and then 5 random image regions of size (128 × 128) pixels were extracted from each image. This is followed by applying the horizontal flip and rotation 5 degrees (e.g., clockwise and counter-clockwise) for every single image in the dataset. Therefore, a total of 24,000 X-ray images of size (128 × 128) pixels were extracted

from both classes (e.g., COVID-19 and normal images). The data augmentation procedure was implemented after dividing the COVID19-vs-normal dataset into three mutually exclusive sets (e.g., training, validation, and testing set) to avoid producing biased detection results.

3.2 Proposed image enhancement procedure

A raw chest X-ray image captured directly using a digital detector have a very poor image quality, which makes it inappropriate for diagnosis and treatment assessment purposes. To enhance the poor quality of the X-ray image, some image enhancement methods should be applied. Furthermore, training the DNNs on top of pre-processed images instead of using raw images data, as a form of supervising the learning process, can significantly enhance the generalization ability of the DNNs and learn more distinctive feature representations with less time needed to obtain the best-trained model. Thus, an efficient image enhancement process is implemented to enhance the poor quality of the X-ray images before feeding them to the proposed deep learning approaches. Firstly, the small details, textures, and low image contrast of the X-ray image was enhanced by applying an adaptive contrast enhancement method using CLAHE (Zuiderveld 1994). CLAHE is different from the original histogram equalization method where several histograms are computed (e.g., each one corresponding to a distinct part of an image) to redistribute the lightness values of the input image, as shown in Fig. 4b. Hence, the CLAHE method can enhance the image local contrast and enhance the visibility of edges and curves in each part of an image. Secondly, the Butterworth
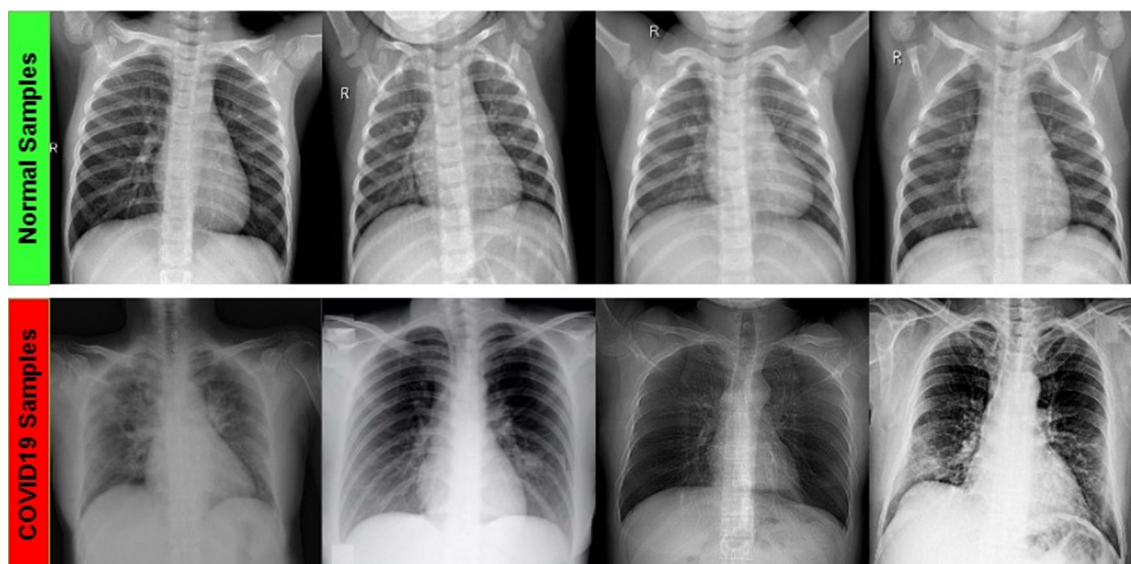
Fig. 3 Some samples of normal and COVID-19 infected cases from the created COVID19-vs-normal dataset
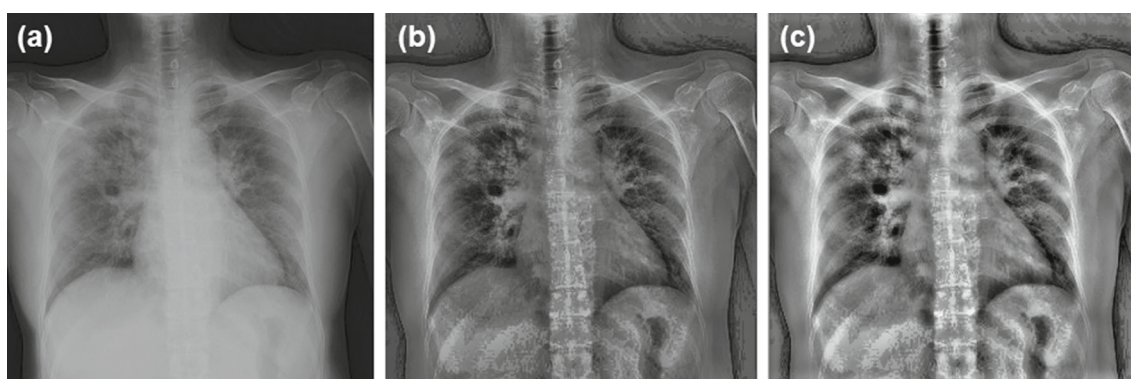
Fig. 4 Proposed image enhancement procedure outputs: **a** A raw X-ray image, **b** applying the CLAHE method, and **c** applying the Butterworth bandpass filter

bandpass filter was applied to eliminate the noise level in the image produced from the previous step, as shown in Fig. 4c. The Butterworth bandpass filter (H_{BP}) was calculated by multiplying the low and high pass filter as follows:

$$H_{LP}(u, v) = \frac{1}{1 + [F(u, v)/F_L]^{2n}} \quad (1)$$

$$H_{HP}(u, v) = 1 - \frac{1}{1 + [F(u, v)/F_H]^{2n}} \quad (2)$$

$$H_{BP}(u, v) = H_{LP}(u, v) * H_{HP}(u, v) \quad (3)$$

where H_{LP} and H_{HP} refer to output of the low and high pass filter, respectively. F_L and F_H are the cut frequencies of the low and high pass filter and set to be 15 and 30, respectively; $n = 3$ is the filter order and is $F(u, v)$ the distance from the origin.

3.3 COVID-19 detection with transfer learning

The transfer learning strategy has been successfully applied to address many deep learning issues arising from the unavailability of sufficient labeled training data. Several studies have proved the advantages of transfer learning in improving the performance of DNNs and solving many challenging problems in computer vision (Lu et al. 2019). In practical applications, rather than training a DNN from scratch, the transfer learning strategy aims to improve their performance by transferring the knowledge (e.g., weights) already learned on a large-scale dataset of a different task to the current task in hand (Shallu and Mehra 2018). This will enable the DNNs to learn general feature representations (e.g., edges, curves, corners, etc.) from the dataset of the initial task that cannot be learned due to the limited amount of the training data in the current task. In this work,

the transfer learning strategy to pre-trained ResNet34 and HRNet model was applied for several reasons, including: (1) to avoid the overfitting problem due to unavailability of sufficient chest X-ray images, especially images with confirmed COVID-19 infection, (2) to reduce the computational complexity during the training process, and (3) to increase the prediction accuracy of the proposed COVID-CheXNet system. The main architecture and implementation details of the employed deep learning models are explained in the next subsections.

3.3.1 ResNet34 model

Herein, transfer learning to the pre-trained ResNet34 model on the ImageNet dataset was applied to improve the accuracy of detecting COVID-19 virus in the X-ray images. The residual network (ResNet) is a powerful deep CNNs (He et al. 2016). ResNet is almost similar to other CNNs models, which have convolutional, pooling, activation maps and fully connected layers stacked sequentially one over the other. The only main difference between the ResNet and the other CNNs models is the identity connection, which links the input layer with the end of the residual block, as shown in Fig. 5b. The ResNet34 architecture starts by performing a convolutional and max-pooling operation using kernels of size (7 × 7) pixels and (3 × 3) pixels, respectively. Afterward, a different number of residual blocks were implemented within four stages, in which trainable kernels of size (3 × 3) pixels were used to perform the convolutional operation, as shown in Table 1. As one moves from one stage to the next one, the channel depth was doubled and the input image size was reduced to half. In this work, the employed ResNet34 model has an average pooling layer followed by one fully connected layer of only two neurons to represent the predicted classes (e.g., normal and COVID-19). In the learning process, the weights of the pre-trained ResNet34 model were used as an initial step, and then they were fine-tuned using Adam optimizer over the current training set. The main idea is that the pre-trained ResNet3 model has a deep knowledge about detecting different types of feature representations (e.g., edges, curves, corners, etc.), and by fine-tuning its parameters this will enable the Resnet34 model to quickly learn the specific feature representations of the current task.

3.3.2 HRNet model

A high-resolution network (HRNet) is a DNN developed by Sun et al. (2019). It starts from high-resolution in the first subnetworks, and then gradually high-to-low resolution subnetworks were added one after another to create more branches. These added multi-resolution subnetworks are connected in parallel. Next, repeated multi-scale
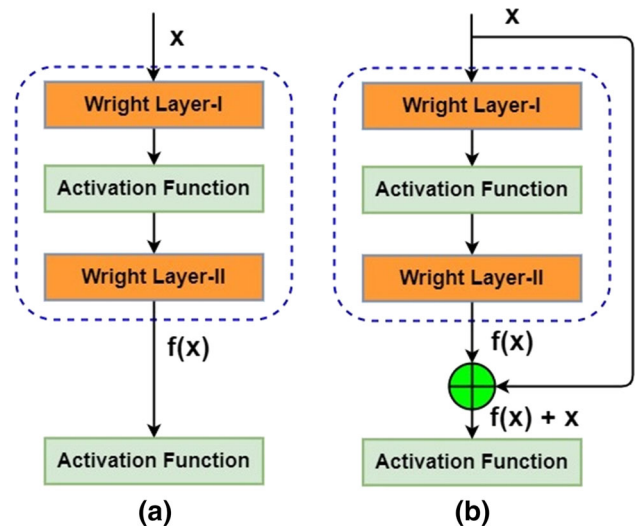

Fig. 5 The difference between: **a** regular block and **b** residual block

Table 1 The ResNet34 architecture details

Layer name	ResNet34
Conv-1	7 × 7, 64 stride 2
Pool-1	3 × 3 Max-Pooling stride 2
Stage-1	[3 × 3, 64 3 × 3, 64] × 3
Stage-2	[3 × 3, 128 3 × 3, 128] × 4
Stage-3	[3 × 3, 256 3 × 3, 256] × 6
Stage-4	[3 × 3, 512 3 × 3, 512] × 3
Pool-2	Average pooling, stride 1
Fc	2-d, Softmax

fusions were implemented to exchange the data between parallel subnetworks in order to strength the high-resolution representations. The HRNet has successfully applied to address many challenging problems in the computer vision field, such as object detection, human pose estimation, semantic segmentation, and facial landmark detection (Sun et al. 2019; 2020a, b; Sun et al. 2019; Cheng et al. 2020). As depicted in Fig. 6, the main architecture of HRNet consists of four stages with four subnetworks connected in parallel. The resolution of these connected subnetworks is gradually decreased to a half while the number of feature maps (channels) is doubled. The first stage consists of four residual blocks where each block was formed by a bottleneck with 64 channels (width). This is followed by applying one convolution operation using kernel of size (3 × 3) pixels to reduce the width of feature maps to $C = 32$. The other three stages consist of (1, 4, and 3) multi-resolution blocks (exchange blocks), respectively. Each exchange block consists of four residual block where each block has two convolutional layers of (3 × 3) pixels
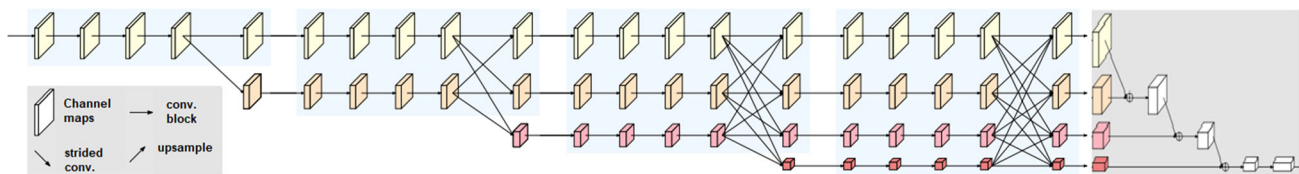
Fig. 6 The main architecture of the HRNet model

in each resolution. In general, there are totally eight exchange blocks, which means eight multi-scale fusions are performed (Wang et al. 2020a, b).

In this work, to perform a classification task, the pre-trained HRNets model on the ImageNet dataset was augmented with a classification head by feeding the four-resolution feature representations of the last stage into a bottleneck and increasing their width (the number of channels) to 128, 256, 512, and 1024, respectively. Then, the high-resolution maps were down-sampled by performing two strided convolutional operations of (3×3) pixels producing 256 width, and they were added to the representations of the second high-resolution representations. The same process was repeated two times to obtained 1024 channels over the small resolution. Finally, a 2048-dimensional vector was generated by performing one convolutional operation of (1×1) pixels to on the top of 1024 channels, followed by an average pooling layer. This last obtained feature vector was fed into the softmax classifier to produce the final decision and assign the input image to one of the predicted classes (e.g., normal and COVID-19).

3.4 Training methodology

To ensure the effectiveness of the proposed training methodology, all of the experiments were conducted by using 70% randomly selected X-ray images as a training set to train the proposed deep learning models (e.g., ResNet34 and HRNet), while the reset 30% were used as a testing set to report the final performance of the best-trained models. During the learning process, 10% was chosen randomly from the training set and employed as a validation set to assess the generalization ability of the model and store the configuration of the weights that produce a minimum error rate on the validation set. The following steps summarized the training methodology of the proposed deep learning models (e.g., ResNet34 and HRNet):

1. Dividing the dataset into a training set, validation set, and test set.
2. Selecting initial values for a set of the hyper-parameters (e.g., momentum, learning rate, weight decay, etc.).

3. Training the network using the training and hyper-parameters sets in 2.
4. Using the validation set to evaluate the performance of the network during the training process.
5. Repeating steps 3 and 4 for 10 epochs.
6. Selecting the best-trained model with the highest validation accuracy rate.
7. Using the testing set to report the real performance of the best-trained model.

3.5 Evaluation criteria

In the prediction phase, the average values of seven quantitative performance measures were computed to assess the reliability of the COVID-CheXNet system using the testing set, including detection accuracy rate (DAR), sensitivity, specificity, precision, F1-score, mean squared error (MSE), and root-mean-squared error (RMSE). These seven quantitative performance measures are calculated as follows:

$$DAR = \frac{(TP + TN)}{(TP + TN + FP + FN)} \tag{4}$$

$$Sensitivity\ (Recall) = \frac{(TP)}{(TP + FN)} \tag{5}$$

$$Specificity = \frac{(TN)}{(TN + FP)} \tag{6}$$

$$Precision = \frac{(TP)}{(TP + FP)} \tag{7}$$

$$F1\ Score = 2 * \frac{(Precision * Recall)}{(Precision + Recall)} \tag{8}$$

Here, TP = true positives, TN = true negatives, FP = false positives, and FN = false negatives.

$$MSE = \frac{1}{n} \sum_{i=1}^{n} (Y_i - \hat{Y}_i)^2 \tag{9}$$

$$RMSE = \sqrt{\frac{1}{n} \sum_{i=1}^{n} (Y_i - \hat{Y}_i)^2} \tag{10}$$

Here, n stands for the total number of data samples, Y the vector of observed values of the variable being predicted, and $\hat{Y}$ being the vector of predicted values.

4 Experimental results

In this section, several extensive experiments on the COVID19-vs-normal dataset were carried out to validate the efficiency of the proposed deep learning models (e.g., ResNet34 and HRNet), along with their combination (e.g., using different fusion rules in the score-level fusion and decision-level fusion) and compare their performances with the current state-of-the-art COVID-19 detection systems. The proposed COVID-CheXNet system code was written using Python programming language and trained on a Google Colaboratory server using Windows 10 operating system, 69 K GPU graphics card, and 16 GB of RAM.

4.1 Training details of deep learning models

The hyper-parameters of the best-trained models (e.g., ResNet34 and HRNet) used in the proposed COVID-CheXNet System are presented in Table 2. As mentioned before, the ResNet34 model was pre-trained on the ImageNet dataset and its weights values fine-tuned on the created COVID19-vs-normal dataset via transfer learning strategy. All the weights were updated using Adam's optimization method along with a learning rate adaptation strategy, in which the learning rate value was decreased by a factor of 0.7 when the learning stagnates during the learning process ('patience policy'). Following the proposed training methodology, the number of epochs, learning rate, momentum value, dropout ratio, and batch size were experimentally set to 10, 0.01, 0.95, 0.5, and 100, respectively. Table 3 shows the values of the training and validation loss beside the time in seconds and accuracy rates for each epoch. From this table, a gradual decrease in both the training and validation loss was observed with a significant increase in the accuracy rate on the validation set. This can be attributed to the generalization ability of the pre-trained ResNet34 to quickly learn more discriminative feature representations from the chest X-ray images. The curve of the loss value against the log scale of the learning rate to find a perfect order of magnitude of the learning rate is shown in Fig. 7. The value that approximately falls in the middle of the sharpest downward slope was selected as the adopted learning rate to train the ResNet34 model.

Following the same training methodology described above, the HRNet model was trained on the top of the COVID19-vs-normal dataset and its weights were updated using SGD optimizer along with a learning rate of 0.01, weight decay of 0.0005, momentum value of 0.9, dropout ratio of 0.5, batch size of 100 and a learning rate adaptation strategy with the power of 0.9 was applied for decreasing the learning rate. Initially, the HRNet model was trained

Table 2 The hyper-parameters of the best-trained models (e.g., ResNet34 and HRNet) used in the proposed COVID-CheXNet system

| ResNet34 model		HRNet model	
Hyper-parameters	Values	Hyper-parameters	Values
Optimizer	Adam	Optimizer	SGD
Momentum	0.95	Momentum	0.9
Weight decay	0.0005	Weight decay	0.0005
Batch size	100	Batch size	100
Dropout	0.5	Dropout	0.5
Learning rate	0.01	Learning rate	0.01
Factor	0.7	Factor	0.9
Patience	5	Patience	5
Total no. of epochs	10	Total no. of epochs	20

Table 3 The values of the training and validation loss beside the time in seconds and accuracy rates for each epoch

Epoch	Train loss	Valid loss	Accuracy	Time (s) per epoch
0	0.33995	0.22055	0.956	04:45
1	0.32598	0.19004	0.957	04:45
2	0.32001	0.14345	0.962	04:45
3	0.28002	0.12234	0.965	04:45
4	0.25577	0.11455	0.971	04:45
5	0.22955	0.10553	0.974	04:45
6	0.19924	0.10455	0.980	04:45
7	0.09404	0.01455	0.985	04:45
8	0.03495	0.00345	0.986	04:45
9	0.01403	0.00155	0.989	04:45

for 10 epochs; however, it was noticed that the performance of the HRNet model can be further advanced by increasing the number of epochs. Hence, the number of epochs was set to around 20 epochs using the early stopping procedure. Figure 8 shows the curve of the loss of the loss value against the batches processed in the training and validation sets for both adopted deep learning models (e.g., ResNet34 and HRNet). From this figure, one can see that the training loss was far higher than validation loss that shows under-fitting. However, with more numbers of batches were processed the curves of both losses become almost equal, which refers to the ideal status of an excellent model.

4.2 Learning useful feature representations

In this section, several extensive experiments were conducted to demonstrate the significant contribution of the
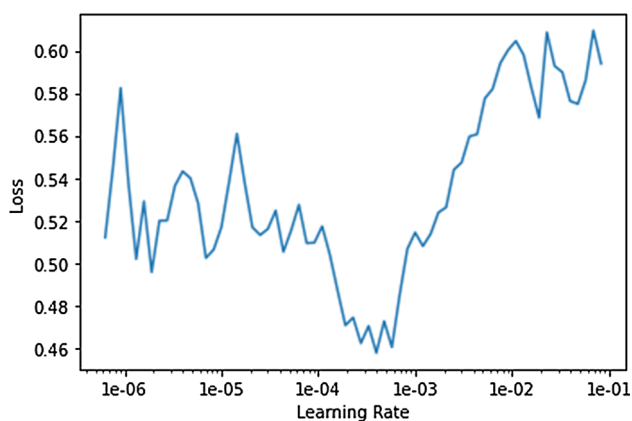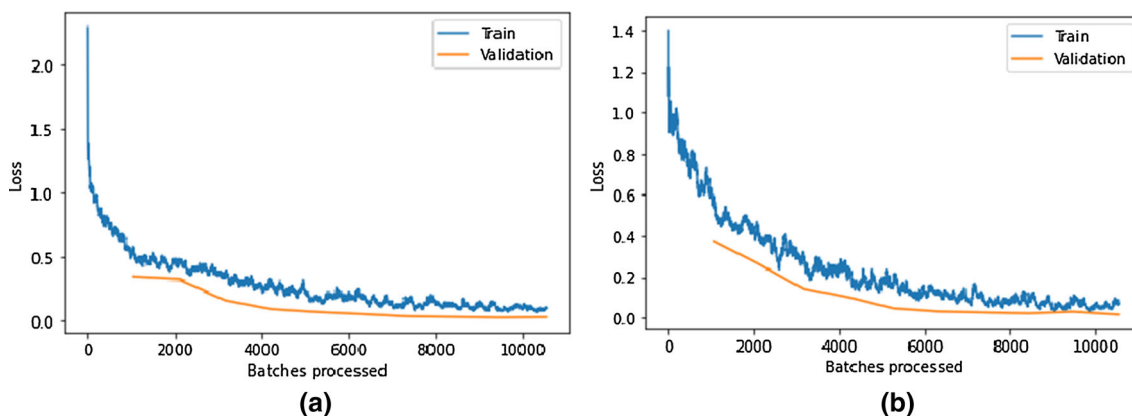
Fig. 7 The curve of the loss against the log scales of the learning rates, to find a perfect order of magnitude of the learning rate

employed image enhancement procedure in guiding the learning process of the adopted deep learning models to learn more powerful and useful feature representations and increasing the DAR of the proposed adopted deep learning models compared with direct use of the raw images data. Firstly, the adopted learning models were separately trained using two different image datasets (e.g., raw images data and pre-processed images data) by following the same training methodology described in (Sect. 3.4). Then, given a total of 7200 X-ray images (e.g., 3600 normal and 3600 positive COVID-19 infected images) in the testing set, the efficiency of the obtained trained models was quantitatively assessed by computing the average values of seven quantitative measures for both classes (e.g., Normal and COVID-19 class). As shown in Table 4, the proposed deep learning models (e.g., ResNet34 and HRNet) have achieved better results by training them on the top of the pre-processed chest X-ray images compared with the direct usage of the raw images data. The ResNet34 model has managed to diagnose the COVID-19 patients with a DAR of 97.02%, sensitivity of 98.41%, specificity of 95.72%, precision of 95.60%, F1-score of 96.98%, MSE of 0.061%,

and RMSE of 0.073%. On the other hand, a DAR of 98.68%, sensitivity of 98.72%, specificity of 98.63%, precision of 98.63%, F1-score of 98.68%, MSE of 0.032%, and RMSE of 0.042% was achieved by the HRNet model using pre-processing images data as an input. It is worthy to mention that the high precision values of 95.60% and 98.63% achieved by ResNet34 and HRNet model, respectively, it is extremely crucial to reduce the number of misclassified healthy cases, as COVID-19 infected cases. Secondly, the ROC curves were plotted by computing the true positive ratio (TPR) and false positive ratio (FPR) for different accuracy thresholds, as shown in Fig. 9. From this figure, one can see that the proposed ResNet34 and HRNet models have managed to achieve an area under the ROC curve (AUC) of 81% and 88% using the raw X-ray images data compared with AUC of 99% and 100% using pre-processing images, respectively.

Finally, the confusion matrices of the normal and COVID-19 infected test results using the adopted deep learning models are shown in Fig. 10. It was observed that using the raw images data as an input to train the ResNet34 model, 770 (9.16%) COVID-19 infected images have misidentified as healthy images and 930 (11.07%) healthy images have misclassified as they containing COVID-19 virus. In contrast, 370 (4.4%) COVID-19 infected images have misidentified as healthy images and 130 (1.54%) healthy images have misclassified as COVID-19 positive cases, by training the ResNet34 model on the top of the pre-processed chest X-ray images. It was found that using the raw images data, the HRNet model has misidentified 730 (8.68%) COVID-19 infected images as healthy images and 950 (11.3%) healthy images as they containing COVID-19 virus, whereas only 115 (1.36%) COVID-19 infected images have misidentified as healthy images and 107 (1.27%) healthy images have misclassified as they containing COVID-19 virus by training the HRNet model on the top of pre-processed images data. In general, a

Fig. 8 The curve of the loss against the batches processed in the training and validation sets: **a** ResNet34 model, and **b** HRNet model

Table 4 The performance evaluation metrics of the proposed deep learning models

Quantitative measures	Raw images		Processed images	
	ResNet34 model	HRNet model	ResNet34 model	HRNet model
DAR	89.88	90.00	97.02	98.68
Sensitivity (recall)	89.14	88.98	98.41	98.72
Specificity	90.66	91.08	95.72	98.63
Precision	90.83	91.31	95.60	98.63
F1-Score	89.98	90.13	96.98	98.68
MSE	0.154	0.121	0.061	0.032
RMSE	0.216	0.136	0.073	0.042
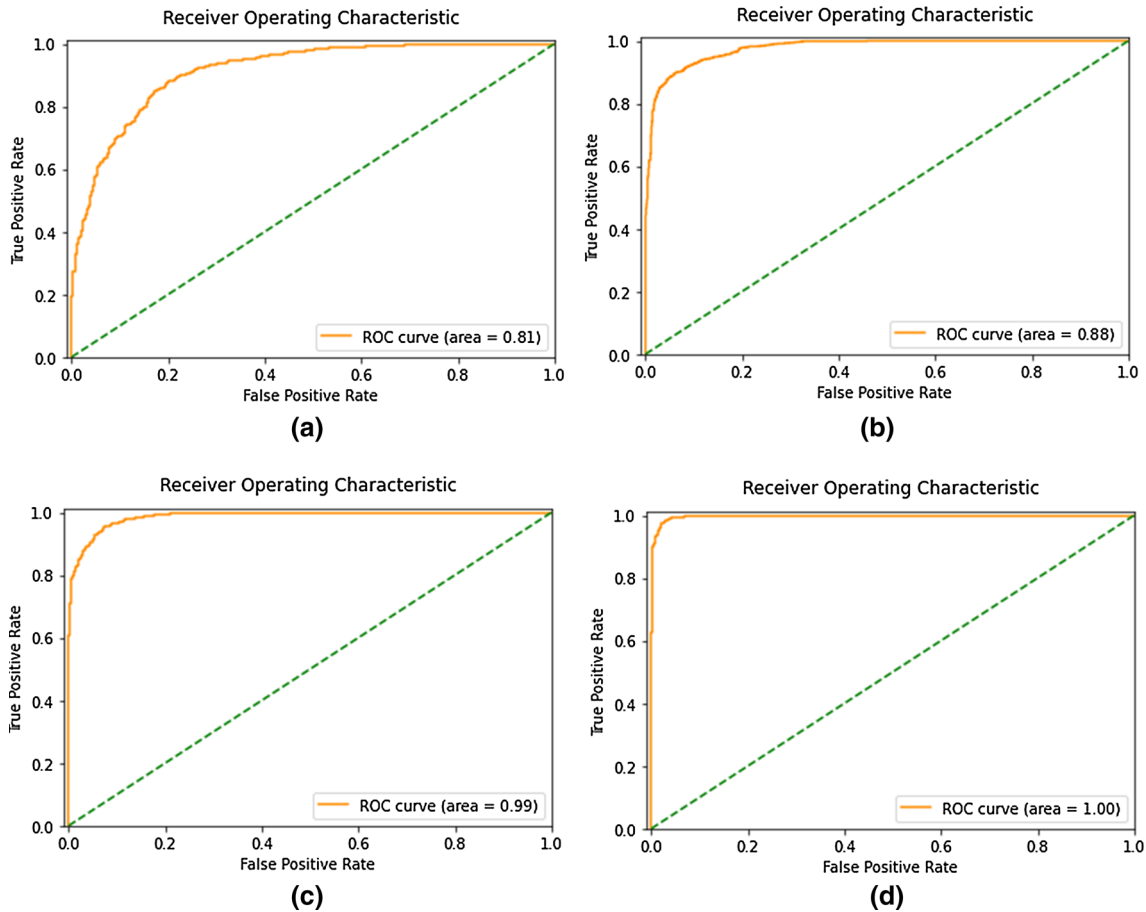
Fig. 9 ROC curves for the proposed deep learning models trained on two different datasets: **a** ResNet34 model trained using raw images, **b** HRNet m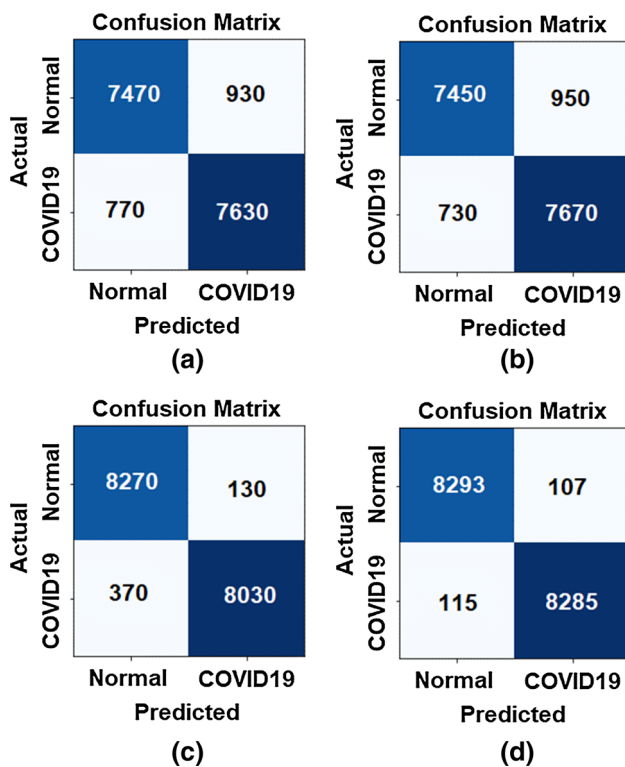odel trained using raw images, **c** ResNet34 model trained using pre-processing X-ray images, and **d**, **c** HRNet model trained using pre-processing X-ray images

slightly better results were obtained using the HRNet model compared with the ResNet34 model.

4.3 Fusion rule evaluation

The final decision of the proposed COVID-CheXNet system is made by combining the results generated from two different deep learning models (e.g., ResNet34 and HRNet). Every time an X-ray image is assigned to the proposed COVID-CheXNet system, two predicted probability scores are computed, and the highest probability score is used to assign the input image to one of two classes (e.g., either normal or COVID-19 class). In this section, the results obtained from the ResNet34 and HRNet models were combined and evaluated using different fusion rules in the score-level fusion (e.g., using sum, weighted sum, product, max, and min rule) and decision-level fusion (e.g., using AND OR rule). Additional information on how these

Fig. 10 Confusion matrices for the proposed deep learning models trained on two different datasets: **a** ResNet34 model trained using raw images, **b** HRNet model trained using raw images, **c** ResNet34 model trained using pre-processing X-ray images, and **d**, **c** HRNet model trained using pre-processing X-ray images

fusion rules are implemented in both levels can be found in (Jain et al. 2007). In the proposed COVID-CheXNet system, the parallel architecture was considered, which provides radiologists a high degree of confidence to make their final decision and to accurately distinguish between healthy and COVID-19 infected subjects. In the implementation of the WSR at the score-level, slightly a higher weight value was given to the HRNet model compared to the ResNet34 model due to a better performance was achieved by the former model compared to the latter. Moreover, no normalization process was required before applying the score fusion rules due to both classifiers are generating the same probability scores and within the same numeric range [0, 1]. Herein, the average values of seven quantitative performance measures using various fusion rules at the score-level and decision-level fusion, are presented in Tables 5 and 6, respectively. A significant enhancement in the accuracy of the proposed hybrid COVID-CheXNet system has been obtained compared with that of using the ResNet34 or HRNet model alone. From Tables 5 and 6, it can be noted that the highest values of the adopted seven quantitative measures were obtained using the WSR and the OR rule in the score-level fusion and decision-level fusion, respectively. The proposed COVID-CheXNet

system can accurately diagnose the patients with COVID-19 in the score-level fusion with a DAR of 99.99%, sensitivity of 99.98%, specificity of 100%, precision of 100%, F1-score of 99.99%, MSE of 0.011%, and RMSE of 0.012% using the WSR and in the decision-level fusion using the OR rule with a DAR of 99.91%, sensitivity of 99.95%, specificity of 99.87%, precision of 99.87%, F1-score of 99.91%, MSE of 0.014%, and RMSE of 0.016%. The high precision value of 100% achieved in the score-level fusion using the WSR is essential in reducing the number of misclassified healthy cases as COVID-19 cases.

Finally, the two confusion matrices of the testing results of for the proposed COVID-CheXNet system using the WSR and OR rule are shown in Fig. 11. It was found that using the WSR in the score-level fusion, only 2 (0.02%) healthy images have been misclassified as if they contain the COVID-19 virus. In contrast, 11 (0.13%) COVID-19 infected images have misclassified as healthy images and 4 (0.04%) healthy images have misclassified as they containing COVID-19 virus using OR rule in the decision-level fusion. Thus, the WSR was used in the performance comparison process of the proposed COVID-CheXNet system with current state-of-the-art systems, due to its effectiveness in exploiting the strength of each classifier compared to other fusion rules. These results obtained have further strengthened our confidence in the possibility of employing the proposed COVID-CheXNet system in real-world settings to significantly moderate the workload of radiologists and help them to accurately detect the COVID-19 infection in the chest X-ray images.

4.4 Comparison study and discussion

The reliability and efficiency of the proposed COVID-CheXNet system were compared with the most current state-of-the-art COVID-19 detection systems. The first three COVID-19 detection systems were evaluated on the COVIDx dataset, which contains only 76 CX-R images with confirmed COVID-19. The first system was developed by Wang and Wong (2020). The authors used a deep tailored designed model based on a CNN, termed as a COVID-Net for detecting the COVID-19 virus in the chest radiography images. The second system was proposed by Farooq and Hafeez (2020). The authors have used a pretrained ResNet50 model, termed as a COVID-ResNet for detecting the COVID-19 in the chest radiography images. The third system was proposed by Luz et al. (2020). The authors have assessed the performance of different architectures of EfficientNet using an updated version of the COVIDx dataset that contains 183 chest radiography images with confirmed COVID-19. The performances of these three systems were evaluated by computing four quantitative measures (e.g., accuracy, sensitivity, precision,

Table 5 Performance comparison of the proposed hybrid COVID-CheXNet using five different rules in score-level fusion

Evaluation criteria	ResNet34	HRNet	Score fusion rules				
			SR	WSR	PR	Max	Min
DAR	97.02	98.68	98.33	99.99	97.99	98.84	97.23
Sens.(recall)	98.41	98.72	98.86	99.98	97.85	98.71	97.62
Specificity	95.72	98.63	97.84	100	97.23	98.64	97.82
Precision	95.60	98.63	97.81	100	97.93	97.98	97.75
F1 Score	96.98	98.68	98.93	99.99	98.82	98.59	97.53
MSE	0.061	0.032	0.099	0.011	0.091	0.052	0.067
RMSE	0.073	0.042	0.034	0.012	0.041	0.047	0.036

Table 6 Performance comparison of the proposed hybrid COVID-CheXNet system using two different rules in decision-level fusion

Evaluation criteria	ResNet34	HRNet	Decision fusion rules	
			AND	OR
DAR	97.02	98.68	97.83	99.91
Sens.(recall)	98.41	98.72	97.76	99.95
Specificity	95.72	98.63	98.78	99.87
Precision	95.60	98.63	98.82	99.87
F1 Score	96.98	98.68	97.84	99.91
MSE	0.061	0.032	0.039	0.014
RMSE	0.073	0.042	0.028	0.016
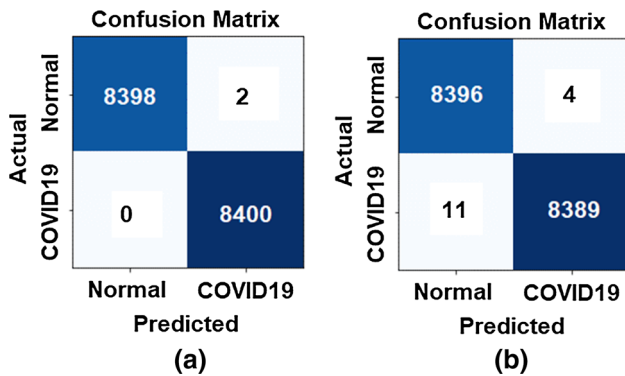
Fig. 11 Confusion matrices for the proposed COVID-CheXNet system using different fusion rules: **a** WSR rule in the score-level fusion, and **b** OR rule in the decision-level fusion

and F1-score) for three different classes (e.g., normal, none-COVID19, and COVID-19). For a fair comparison, the average value of these four quantitative measures was adopted and is shown in Table 7. It can be seen that the proposed COVID-CheXNet system obtains better results compared with these three COVID-19 detection systems. Although the EfficientNet-B3 model described in (Luz et al. 2020) achieved the same precision of 100%, the proposed COVID-CheXNet system has managed to produce better results on the other two terms (e.g., accuracy and sensitivity) using a larger dataset containing more chest X-ray images with confirmed COVID-19. Another comparison study between three different CNN models (e.g., ResNet50, InceptionV3, and Inception-ResNetV2) was presented by Narin et al. (2020) to detect COVID-19 infected patients using chest X-ray images. The authors calculated the mean values of five different quantitative measures (e.g., accuracy, recall, specificity, precision, and F1-score) using a fivefold cross-validation procedure to assess the performance of the three adopted models. The best performance was obtained using the pre-trained ResNet50 model with a DAR of 98%, sensitivity of 96%, specificity of 100%, precision of 100%, and F1-score of 98%. Although the ResNet50 model has achieved the same specificity and precision compared with the proposed COVID-CheXNet system, it achieved inferior results in terms of other quantitative measures, as shown in Table 8.

These findings confirm the usefulness of the proposed image enhancement procedure as well as the transfer learning strategy to improve the prediction accuracy of the proposed COVID-CheXNet system by successfully

Table 7 Performance comparison between the proposed COVID-CheXNet system and three current state-of-the-art COVID-19 detection systems evaluated on the COVIDx dataset

Quantitative measures	Proposed COVID-CheXNet system	COVID-Net (Wang and Wong 2020)	COVID-ResNet (Farooq and Hafeez 2020)	EfficientNet-B3 (Luz et al. 2020)
Accuracy	99.99	92.4	96.23	93.9
Sens. (recall)	99.98	88.6	96.92	96.8
Precision	100	91.3	96.86	100
F1 Score	99.99	–	96.88	–

Table 8 Performance comparison between the proposed COVID-CheXNet system and ResNet50 (Narin et al. 2020)

Quantitative measures	Proposed COVID-CheXNet system	ResNet50 model (Narin et al. 2020)
Accuracy	99.99	98
Sens.(recall)	99.98	96
Specificity	100	100
Precision	100	100
F1-Score	99.99	98

transferring the knowledge from the source dataset (ImageNet) to the current task despite the small size of chest X-ray images dataset. In addition to the possibility of employing the COVID-CheXNet system in real-world clinical settings to reduce the pressure on the radiologists in clinical practice, with less than 2 s per image required to obtain the prediction result. Although the proposed COVID-CheXNet system has managed to achieve satisfying performance with a DAR of 99.99%, it is limited to classify the input chest X-ray image into only two classes either normal or COVID-19. Thus, the number of predicted classes can be extended by adding chest X-ray images with other types of pneumonia (e.g., bacterial pneumonia and viral pneumonia). Further experiments need to be conducted using a large scale dataset with more chest X-ray images with confirmed COVID-19 infection to prove the effectiveness of the proposed COVID-CheXNet system.

5 Conclusions and future work

This study has investigated the potential of using some efficient image processing and deep learning approaches to build an accurate and real-time diagnostic system, termed as COVID-CheXNet system for COVID-19 virus in the X-rays images. Using the proposed COVID-CheXNet system, the poor image quality was enhanced and the noise level was reduced by applying the CLAHE method and Butterworth bandpass filter, respectively. Then, two discriminate deep learning models (e.g., ResNet34 and HRNet) were trained on the top of the pre-processed chest radiography images to increase the generalization ability of the last trained model and avoid the overfitting problem. The performance of the COVID-DeepNet system was tested by creating a large-scale X-ray images dataset, termed as the COVID19-vs-normal dataset. The proposed COVID-CheXNet system has managed to achieve comparable performance with expert radiologists with a DAR of 99.99%, sensitivity of 99.98%, specificity of 100%, precision of 100%, F1-score of 99.99%, MSE of 0.011%,

and RMSE of 0.012% using the WSR in the score-level fusion. This research could alleviate the pressure on decision-makers (e.g., radiologists and clinicians) caused by the increased number of COVID-19 patients compared with the shortage of medical resources. Further experiments will be required to prove the efficacy and accuracy of the proposed COVID-CheXNet system by using a larger and more challenging dataset contains more chest X-ray images with conformed COVID-19 infection and other types of pneumonia (e.g., bacterial pneumonia and viral pneumonia). This is an important and vital issue for future research.

Compliance with ethical standards

Conflict of interest The authors declare that they have no conflict of interest.

Ethical approval This article does not contain any studies with human participants or animals performed by any of the authors.

References

Al-Waisy AS et al (2017a) A multimodal deep learning framework using local feature representations for face recognition. Mach Vis Appl 29(1):35–54. https://doi.org/10.1007/s00138-017-0870-2

Al-Waisy AS et al (2017b) A multimodal biometric system for personal identification based on deep learning approaches. In: 2017 Seventh international conference on emerging security technologies (EST). pp 163–168

Al-Waisy AS et al (2018) A multi-biometric iris recognition system based on a deep learning approach. Pattern Anal Appl 21(3):783–802. https://doi.org/10.1007/s10044-017-0656-1

Brady AP (2017) Error and discrepancy in radiology: inevitable or avoidable? Insights Imaging 8(1):171–182. https://doi.org/10.1007/s13244-016-0534-1

Castillo O, Melin P (2020) Forecasting of COVID-19 time series for countries in the world based on a hybrid approach combining the fractal dimension and fuzzy logic. Chaos Solitons Fractals Interdiscip J Nonlinear Sci Nonequilib Complex Phenom 140:110242. https://doi.org/10.1016/j.chaos.2020.110242

Chen N et al (2020) Epidemiological and clinical characteristics of 99 cases of 2019 novel coronavirus pneumonia in Wuhan, China: a descriptive study. Lancet 395(10223):507–513. https://doi.org/10.1016/S0140-6736(20)30211-7

Cheng B et al (2020) HigherHRNet: scale-aware representation learning for bottom-up human pose estimation. pp 5385–5394. https://doi.org/10.1109/cvpr42600.2020.00543

Cohen JP, Morrison P, Dao L (2020) COVID-19 image data collection. https://github.com/ieee8023/covid-chestxray-dataset, https://arxiv.org/abs/2003.11597

Dansana D et al (2020) Early diagnosis of COVID-19-affected patients based on X-ray and computed tomography images using deep learning algorithm. Soft Comput. https://doi.org/10.1007/s00500-020-05275-y

De Fauw J et al (2018) Clinically applicable deep learning for diagnosis and referral in retinal disease. Nat Med 24(9):1342–1350. https://doi.org/10.1038/s41591-018-0107-6

Farooq M, Hafeez A (2020) COVID-ResNet: a deep learning framework for screening of COVID19 from radiographs. arXiv preprint https://arxiv.org/abs/2003.14395

Ghoshal B, Tucker A (2020) Estimating uncertainty and interpretability in deep learning for Coronavirus (COVID-19) detection, pp 1–14. arXiv preprint https://arxiv.org/abs/2003.10769.

Gozes O et al (2020) Rapid AI development cycle for the Coronavirus (COVID-19) pandemic: initial results for automated detection and patient monitoring using deep learning CT image analysis, pp 1–19. arXiv preprint https://arxiv.org/abs/2003.05037

Guo H et al (2020) The impact of the COVID-19 epidemic on the utilization of emergency dental services. J Dental Sci. https://doi.org/10.1016/j.jds.2020.02.002

He K et al (2016) Deep residual learning for image recognition. In: Proceedings of the IEEE computer society conference on computer vision and pattern recognition. pp 770–778. http://doi.org/https://doi.org/10.1109/CVPR.2016.90.

Hemdan EE-D, Shouman MA, Karar ME (2020) COVIDX-Net: a framework of deep learning classifiers to diagnose COVID-19 in x-ray images. arXiv preprint https://arxiv.org/abs/2003.11055

Huang C et al (2020) Clinical features of patients infected with 2019 novel coronavirus in Wuhan, China. The Lancet 395(10223):497–506. https://doi.org/10.1016/S0140-6736(20)30183-5

Italian Society of Medical and Interventional Radiology (SIRM): (2020) https://www.sirm.org/en/italian-society-of-medical-and-interventional-radiology/. Accessed: May 11 2020

Jain A, Flynn P, Ross AA (2007) Handbook of biometrics. Springer, Berlin. https://doi.org/10.1007/978-0-387-71041-9

Kaggle's Chest X-Ray Images (Pneumonia) dataset: (2020) https://www.kaggle.com/paultimothymooney/chest-xray-pneumonia. Accessed May 11 2020

Kassani SH et al (2020) Automatic detection of coronavirus disease (COVID-19) in X-ray and CT images: a machine learning-based approach, pp 1–18. arXiv preprint https://arxiv.org/abs/2004.10641

Kumar P, Kumari S (2020) Detection of coronavirus disease (COVID-19) based on deep features. http://doi.org/10.20944/preprints202003.0300.v1

Lu S, Lu Z, Zhang YD (2019) Pathological brain detection based on AlexNet and transfer learning. J Comput Sci 30:41–47. https://doi.org/10.1016/j.jocs.2018.11.008

Luz E et al (2020) Towards an effective and efficient deep learning model for COVID-19 patterns detection in X-ray images, pp 1–10. arXiv preprint https://arxiv.org/abs/2004.05717.

Melin P et al (2020) Analysis of spatial spread relationships of Coronavirus (COVID-19) pandemic in the world using self organizing maps. Chaos Solit Fract

Mohammed MA et al (2020) Benchmarking methodology for selection of optimal COVID-19 diagnostic model based on entropy and TOPSIS methods. IEEE Access 8(1):1–17. https://doi.org/10.1109/ACCESS.2020.2995597

Narin A, Kaya C, Pamuk Z (2020) Automatic detection of coronavirus disease (COVID-19) using X-ray images and deep convolutional neural networks. arXiv preprint arXiv:2003.10849

Ng MY, Lee EY, Yang J, Yang F, Li X, Wang H, Lui MM, Lo CS, Leung B, Khong PL (2020) Imaging Profile of the COVID-19 infection: radiologic findings and literature review. Radiol Cardiothorac Imaging 2(1):1–8. https://doi.org/10.14358/PERS.80.2.000

Ozturk T et al (2020) Automated detection of COVID-19 cases using deep neural networks with X-ray images. Comput Biol Med. https://doi.org/10.1016/j.compbiomed.2020.103792

Radiological Society of North America (RSNA) (2020) https://www.kaggle.com/c/rsna-pneumonia-detection- challenge/data. Accessed May 11 2020

Radiopaedia dataset (2020) https://radiopaedia.org/search?lang=us&q=covid&scope=cases#collapse-by-diagnostic-certainties. Accessed May 11, 2020

Shallu and Mehra R (2018) Breast cancer histology images classification: Training from scratch or transfer learning? ICT Express 4(4):247–254. https://doi.org/10.1016/j.icte.2018.10.007

Sun K, Xiao B et al (2019) Deep high-resolution representation learning for human pose estimation. In: Proceedings of the IEEE computer society conference on computer vision and pattern recognition, pp 5686–5696. http://doi.org/https://doi.org/10.1109/CVPR.2019.00584

Sun K, Zhao Y et al (2019) High-resolution representations for labeling pixels and regions. Available at: https://arxiv.org/abs/1904.04514

Wang L, Wong A (2020) COVID-Net: a tailored deep convolutional neural network design for detection of COVID-19 cases from chest radiography images. arXiv preprint https://arxiv.org/abs/2003.09871

Wang J et al (2020a) Deep high-resolution representation learning for visual recognition. IEEE Trans Pattern Anal Mach Intell. https://doi.org/10.1109/tpami.2020.2983686

Wang W et al (2020b) Detection of SARS-CoV-2 in different types of clinical specimens. J Am Med Assoc. https://doi.org/10.1001/jama.2020.3786

Worldmeter (2020) https://www.worldometers.info/coronavirus/worldwide-graphs/. Accessed 6 June 2020

Zhang J et al (2020) COVID-19 screening on chest X-ray images using deep learning based anomaly detection. arXiv preprint https://arxiv.org/abs/2003.12338

Zuiderveld K (1994) Realization of the contrast limited adaptive histogram equalization (CLAHE) for real-time image enhancement. Graphic Gems. https://doi.org/10.1023/B:VLSI.0000028532.53893.82

Affiliations

Alaa S. Al-Waisy[1] ⓘ · **Shumoos Al-Fahdawi[2]** ⓘ · **Mazin Abed Mohammed[3]** ⓘ · **Karrar Hameed Abdulkareem[4]** ⓘ ·
Salama A. Mostafa[5] ⓘ · **Mashael S. Maashi[6]** ⓘ · **Muhammad Arif[7]** · **Begonya Garcia-Zapirain[8]**

[1] Communications Engineering Techniques Department, Information Technology Collage, Imam Ja'afar Al-Sadiq University, Baghdad, Iraq

[2] Computer Science Department, Al-Ma'aref University College, Anbar, Iraq

[3] College of Computer Science and Information Technology, University of Anbar, 11, Ramadi, Anbar, Iraq

4   College of Agriculture, Al-Muthanna University,
     Samawah 66001, Iraq

5   Faculty of Computer Science and Information Technology,
     University Tun Hussein Onn Malaysia, 86400 Batu Pahat,
     Johor, Malaysia

6   Software Engineering Department, College of Computer and
     Information Sciences, King Saud University, Riyadh 11451,
     Saudi Arabia

7   School of Computer Science, Guangzhou University,
     Guangzhou, China

8   eVIDA Lab, The University of Deusto, Avda/Universidades
     24, 48007 Bilbao, Spain